

DECODING NATURAL IMAGES FROM EEG FOR OBJECT RECOGNITION

Yonghao Song¹, Bingchuan Liu¹, Xiang Li¹, Nanlin Shi¹, Yijun Wang², Xiaorong Gao^{1*}

¹ Department of Biomedical Engineering, Tsinghua University

² Institute of Semiconductors, CAS

gxr-dea@tsinghua.edu.cn

ABSTRACT

Electroencephalogram (EEG) is a brain signal known for its high time resolution and moderate signal-to-noise ratio. Whether natural images can be decoded from EEG has been a hot issue recently. In this paper, we propose a self-supervised framework to learn image representations from EEG signals. Specifically, image and EEG encoders are first used to extract features from paired image stimuli and EEG responses. Then we employ contrastive learning to align these two modalities by constraining their similarity. Additionally, we introduce two plug-in-play modules that capture spatial correlations before the EEG encoder. Our approach achieves state-of-the-art results on the most extensive EEG-image dataset, with a top-1 accuracy of 15.6% and a top-5 accuracy of 42.8% in 200-way zero-shot tasks. More importantly, extensive experiments analyzing the temporal, spatial, spectral, and semantic aspects of EEG signals demonstrate good biological plausibility. These results offer valuable insights for neural decoding and real-world applications of brain-computer interfaces. The code will be released on <https://github.com/eeyhsong/NICE-EEG>.

1 INTRODUCTION

Our daily life relies on accurately and rapidly identifying objects in complex visual environments (DiCarlo & Cox, 2007). Studies have attempted to decode natural images from brain activities to understand our brain better and construct friendly brain-computer interfaces (Kamitani & Tong, 2005; Kay et al., 2008; Gao et al., 2021). Many studies use functional magnetic resonance imaging (fMRI), recording blood oxygen level-dependent, to classify the objects seen by the human (Du et al., 2023; Horikawa & Kamitani, 2017). Some works further utilize deep learning to reconstruct the image with large-scale datasets and achieve exquisite results (Allen et al., 2022; Gu et al., 2022). Although with high spatial resolution, fMRI commonly requires several seconds for a stable response to one image, which can hardly satisfy the real-time interaction in our life (Fang et al., 2020; Lin et al., 2022). Magnetoencephalogram (MEG) with a high sampling rate has been used for this purpose but is still limited by high cost and large devices (Cichy et al., 2014; Hebart et al., 2023).

People also turn to Electroencephalogram (EEG) for decoding images from visual-evoked brain representation (Spampinato et al., 2017). EEG has high time resolution, low cost, and good portability, but the low signal-to-noise ratio takes some problems (Pan et al., 2022; Kobler et al., 2022). Some works achieve great classification results and capture saliency maps with EEG signals (Palazzo et al., 2021). However, its flawed block-design experiments place images of the same classes in one block, leading to classification with block-level temporal correlation, rather than stimulus-related activity (Li et al., 2021). Some works attain above-chance performance but with the data of a single subject (Ahmed et al., 2021). Besides, the available dataset usually contains only a limited number of categories, which seems insufficient for real image recognition. The latest study collected a large-scale EEG dataset with 16740 image stimuli of 1854 concepts by rapid serial visual presentation (Gifford et al., 2022; Hebart et al., 2019). Despite demonstrating the feasibility of image-to-EEG encoding and category separability, this work analyzed the electrodes on the occipital and parietal regions, which neglects the neuroscience principle that the inferior temporal cortex processes object recognition (Dapello et al., 2023). In addition, the work focuses on the peak of pairwise decoding about 110 ms after stimuli onset. Generally, this duration involves visual conduction and primary

visual processing by a large margin, not semantic understanding. In short, the issues of multi-class image decoding and biological plausibility need to be further addressed.

Pattern recognition strategy is an essential constraint to EEG analysis. Existing work usually performs supervised learning on limited data from a few categories (Cheng et al., 2022). Direct use of machine learning methods such as support vector machines and deep neural networks are not well suited for complex tasks (Fu et al., 2022; Liu et al., 2021). Researchers have also tried to transfer knowledge from other domains, such as the data from different subjects and multi-modal features (Du et al., 2022; Zhao et al., 2021; Du et al., 2023). Actually, multi-modal learning has yielded fantastic performance in computer vision (Wang et al., 2022; Saharia et al., 2022). Natural language supervision could pre-train a visual model while achieving good zero-shot results on downstream tasks (Radford et al., 2021). Moreover, image text pairs replace the original hard labels to drive self-supervised learning for better feature representation. On this basis, we are curious about if information from other modalities could significantly help decode image information from EEG signals. Another problem is the inadequate capability of commonly used EEG feature extractors, which consist of convolutional layers along temporal and spatial dimensions separately (Schirrmester et al., 2017; Lawhern et al., 2018; Song et al., 2023). Raw EEG data is typically organized into two dimensions, i.e., temporal and spatial dimensions encompassing all electrode channels. But the practice disrupts the correlation between channels, which is crucial for brain activity (Ding et al., 2023).

To address the above limitations, we propose a self-supervised framework to decode image representation from EEG signals for object recognition. Specifically, contrastive learning is leveraged to bridge image stimuli and EEG responses. We feed image-EEG pairs to the model and process them by an image encoder and an EEG encoder separately, in which the image encoder has been pre-trained with other image datasets. We then use the cosine similarity between image features and EEG features as a constraint to align the two modalities. After training, we can decode EEG in a zero-shot manner, classifying image categories not seen in the training phase. Furthermore, we perform comparative experiments from different perspectives, including spatial, temporal, and spectral domains, as well as semantic similarity. Explanations are given consistent with neuroscientific knowledge, thus demonstrating the feasibility of EEG-based image decoding. Finally, two plug-in-play tricks are given for better retaining channel correlations with self-attention and graph attention.

Our main contributions can be summarized as follows:

- We propose a self-supervised framework for EEG-based image decoding with contrastive learning. Remarkable zero-shot performance has been achieved on large-scale datasets.
- We further demonstrate the feasibility of investigating natural image information from EEG signals. Comprehensive experiments and analyses show reliable biological plausibility, which brings a new pathway to visual brain-computer interfaces.
- We design two plug-in-play modules with self-attention and graph attention, which can be used to capture spatial correlations between EEG electrode channels.

2 RELATED WORKS

Decoding visual information from our brain has been active in neuroscience and computer science for many years (Miyawaki et al., 2008; Jia et al., 2021). Although some steady-state visual stimuli can be well identified, accurate and fast decoding of natural images remains a challenging problem (Shi et al., 2023). fMRI has been widely used to estimate semantic and shape information from visual processing in our brain (Ho et al., 2023; Takagi & Nishimoto, 2023). However, the high speed and convenience drive this technology toward real scenarios of brain-computer interaction. EEG has gained attention as an alternative to fMRI due to its high temporal resolution and portability (Willett et al., 2021). But general performance on different subjects and biological plausibility remain unsolved (Ahmed et al., 2021). From another perspective, previous work has typically relied on supervised learning methods with limited categories of images for classification (Shen et al., 2019; Li et al., 2021; Liu et al., 2023). These methods focus on separate categories and overlook the intrinsic representation between image stimuli and brain responses. There is still a distance to be used in natural scenarios because they cannot usually generalize to new categories. Motivated by these challenges, we present an EEG-based image decoding framework that employs self-supervised contrastive learning, which helps the model achieve zero-shot generalization in object recognition tasks.

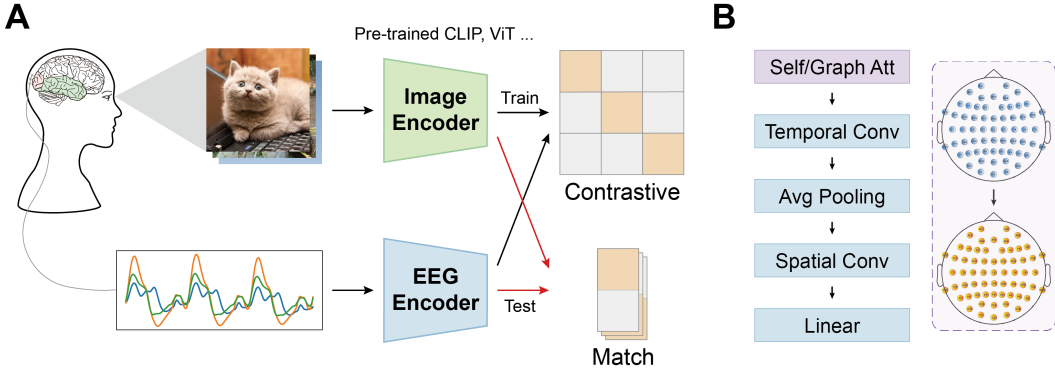


Figure 1: (A) Overall framework based on contrastive learning. During training, image-EEG pairs are input and processed by an image encoder (pre-trained) and an EEG encoder. The similarity of matched pairs is increased, and of unmatched pairs is decreased. During testing, a few images of target categories or concepts that have not been seen are processed in advance into templates. Then the model gives matched results by similarity. (B) Architecture of the EEG encoder. Commonly temporal-spatial convolution is used. The final linear layer transforms the outputs to the same size as the image features. We also design two tricks based on self-attention and graph attention to capture spatial information between electrode channels before the original EEG encoder.

3 METHODS

3.1 OVERVIEW

We propose a contrastive learning-based framework, Natural Image Contrast EEG (NICE), to decode images from EEG. The overall framework is depicted in Fig. 1(A).

In the training process, image and EEG signals are input into the framework as stimulus-response pairs. Subsequently, the image encoder and EEG encoder are used to extract the features of the image and EEG, respectively. Contrastive learning is applied to the same size outputs to align the image and EEG modal representations. The objective of the training is to improve the similarity of matched pairs and reduce that of unmatched pairs. The self-supervised strategy allows the model to learn common information between the two modalities, rather than the traditional supervised learning with labels. Before the test process, we look for a few images that belong to the image concepts to be classified, and have not appeared in the EEG collection experiments. These images are processed by the image encoder and averaged to obtain one template for each concept. Then the test EEG signal is processed by the EEG encoder and calculates similarity with all concept templates. The similarity is used as the matching criterion to determine the decoding results.

We adopt temporal-spatial convolution (TSConv), following the way widely used in EEG analysis, to be the EEG encoder as Fig. 1(B). We also design two plug-in-play "spatial filters" with self-attention and graph attention (Dosovitskiy et al., 2021; Veličković et al., 2018). The correlation between EEG electrode channels is better preserved with these two tricks. It's worth noting that the image encoder we used has been pre-trained on other image datasets. The leading studies in computer vision help us with large sample space, while we cannot easily collect numbers of brain signals in practice.

3.2 NETWORK ARCHITECTURE

3.2.1 EEG ENCODER

Researchers usually arrange the raw EEG trials into two dimensions $C \times T$, in which C denotes electrode channels, and T denotes time samples. Convolution along the two dimensions is widely used in deep learning-based EEG analysis models. In the same way, we present a very concise network architecture as shown in Table 1. One-dimension convolution is first applied to capture the temporal features with k kernels of size $(1, m_1)$ and stride of $(1, 1)$. An average pooling layer with

Table 1: Architecture of EEG encoder with SA or GA followed by TSCConv

Layer	In	Out	Kernel	Stride	Dimension
SA & GA					$[(b, 1, C, T) \rightarrow (b, 1, C, T)]$, b is batch
Temporal Conv	1	k	$(1, m_1)$	$(1, 1)$	$(b, k, C, T - m_1 + 1)$
Avg Pooling	k	k	$(1, m_2)$	$(1, s_2)$	$(b, k, C, (T - m_1 - m_2 + 1)/s_1 + 1)$
Spatial Conv	k	k	$(C, 1)$	$(1, 1)$	$(b, k, 1, (T - m_1 - m_2 + 1)/s_1 + 1)$
Flatten&Linear					$[k * ((T - m_1 - m_2 + 1)/s_1 + 1) \rightarrow \text{shape of image feature}]$

a kernel size of $(1, m_2)$ and stride of $(1, s_2)$ is introduced to alleviate overfitting and smooth the temporal features. Another one-dimension convolution is then used for spatial features keeping k kernels of size $(ch, 1)$ and stride of $(1, 1)$, where ch usually equals the number of electrodes. After each convolutional layer, batch normalization and exponential linear units (ELU) activation functions are used for better training and nonlinearity (Clevert et al., 2016). We can adjust the convolution part to ensure the output scale approximates the image features. Finally, a linear layer is added as a projector to transform the features to the same size as the output of the image encoder.

3.2.2 IMAGE ENCODER

The image features are extracted with the paired EEG features for contrastive learning. There have been some excellent computer vision models that can obtain image features with semantic discrimination. We prefer directly using models pre-trained on other image datasets to get a large sample space. The feature extraction parts of Contrastive Language-Image Pre-training (CLIP) (Radford et al., 2021), Vision Transformer (ViT) (Dosovitskiy et al., 2021), and Residual Neural Networks (ResNet) (He et al., 2016) are tried separately in our framework for demonstration. All the images for stimuli can be processed in advance, thus speeding up our model training.

3.2.3 CONTRASTIVE LEARNING

A concise framework is constructed with contrastive learning, shown in Algorithm 1. The outputs of the image encoder and EEG encoder are normalized separately. Then the dot product is used to evaluate the cosine similarity of all image-EEG feature pairs. A scaled temperature parameter is used to adjust distribution probability during training. Cross entropy loss is employed as the objective function to increase the similarities between matched pairs and decrease the similarities between unmatched pairs. After adequate training, the EEG encoder can extract representations similar to corresponding images. The self-supervised strategy allows us to learn inherent patterns from EEG signals without labels, rather than directly separate different classes with supervised learning.

Algorithm 1 Natural Image Contrast EEG framework

```

1: Input: (Image, EEG) - stimulus & Response
2: Model: Image_encoder - CLIP & EEG_encoder - TSCConv

3: # E - (batch, channel, electrode, sample)                                ▷ batch of input EEG
4: # I - (batch, channel, height, width)                                    ▷ batch of input images
5: # t - learned temperature parameter

6: # extract normalized representations from the raw image and EEG
7: E_f = Norm(Linear(Eeg_encoder(E)))
8: I_f = Norm(Image_encoder(I))                                           ▷ can be obtained before training

9: # scaled pairwise cosine similarity
10: logits = dot(E_f, I_f.T) * exp(t)

11: # symmetric loss function
12: labels = arange(batch)
13: loss_e = cross_entropy_loss(logits, labels, axis=0)
14: loss_i = cross_entropy_loss(logits, labels, axis=1)
15: loss = (loss_e + loss_i) / 2

```

3.3 PLUG-IN-PLAY MODULE

3.3.1 SELF-ATTENTION

The electrode channel connectivity plays a vital role in reflecting spatial information. However, the commonly used arrangement of EEG data corrupts the original correlations. Therefore, we utilize two approaches, self-attention and graph attention, to design plug-in-play modules that can be applied before the EEG encoder as "spatial filters" to encapsulate electrode correlations. We use self-attention (SA) on the electrode channels to evaluate the spatial correlations of EEG data (Vaswani et al., 2017). The input $x_{in} \in \mathbb{R}^{C \times T}$ is linearly transformed into equal-sized weight metrics W_q, W_k, W_v :

$$x'_{in} = \text{Softmax}\left(\frac{W_q x_{in} \cdot (W_k x_{in})^T}{\sqrt{d}}\right) \cdot W_v x_{in} \quad (1)$$

where $x'_{in} \in \mathbb{R}^{C \times T}$ denotes the output after the SA module, d , the time length of EEG data, is a scaled factor to accommodate the Softmax function. Residual connection is employed by integrating the input and output of the SA module, contributing to stable training. (He et al., 2016).

3.3.2 GRAPH ATTENTION

We design another module to update each electrode with all the other channels inspired by (Veličković et al., 2018). We treat each electrode as a node $n_i \in \mathbb{R}^{1 \times T}$, $i = 1, \dots, ch$, which has edges to all the other electrodes \mathcal{N}_i . The process to update one electrode is as follows:

$$n'_i = \alpha_{i,i} W n_i + \sum_{j \in \mathcal{N}_i} \alpha_{i,j} W n_j \quad (2)$$

where n'_i denotes each node after processing, $\alpha_{i,j}$ is attention coefficients indicating importance of node j features to node i , and W is the weight of linear transformation. Calculate $\alpha_{i,j}$ as:

$$\alpha_{i,j} = \frac{\exp(\text{LeakyReLU}(a^T [W n_i \parallel W n_j]))}{\sum_{k \in \mathcal{N}_i \cup \{i\}} \exp(\text{LeakyReLU}(a^T [W n_i \parallel W n_k]))} \quad (3)$$

where a denotes a feedforward layer, $()^T$ is the transposition operator, and \parallel is the concatenation operator. LeakyReLU with a slope of 0.2 is used for nonlinearity in attention calculation.

4 EXPERIMENTS AND RESULTS

4.1 DATASETS AND PREPROCESSING

Large-scale EEG datasets with high time resolution give us a good chance to evaluate our framework (Gifford et al., 2022). The dataset contains data from ten participants with a time-efficient rapid serial visual presentation (RSVP) paradigm. The training set includes 1654 concepts \times 10 images \times 4 repetitions. The test set includes 200 concepts \times 1 image \times 80 repetitions. Images for training and testing appear in a pseudo-randomized order, and a target image is used to reduce eye blinks and other artifacts. Each image displays 100 ms, followed by a 100 ms blank screen. Raw EEG data filtered to [0.1, 100] Hz has 64 channels and a sample rate of 1000 Hz.

For preprocessing, we epoched EEG data into trials ranging from 0 to 1000 ms after stimuli onset. Baseline correction was performed with the mean of 200 ms pre-stimulus data. All electrodes were preserved for analysis with down-sampling to 250 Hz, and multivariate noise normalization was performed with training data (Guggenmos et al., 2018). We averaged all EEG repetitions of one image to ensure the signal-to-noise ratio and compared the impact of repetitions. Images were resized to 224×224 and normalized before being processed by the image encoder.

4.2 EXPERIMENT DETAILS

Our method is implemented with PyTorch in Python 3.10 on a Geforce 4090 GPU. We randomly select 740 trials from 16540 training data as the validation set in each run of our code. Best models are saved when the validation loss reaches a minimum of 200 epochs in the training process. We compute

Table 2: Overall performance of 200-way zero-shot classification: top-1 and top-5

Method	Subject 1		Subject 2		Subject 3		Subject 4		Subject 5		Subject 6		Subject 7		Subject 8		Subject 9		Subject 10		Ave	
	top-1	top-5	top-1	top-5	top-1	top-5	top-1	top-5	top-1	top-5	top-1	top-5	top-1	top-5	top-1	top-5	top-1	top-5	top-1	top-5	top-1	top-5
Subject dependent - train and test on one subject																						
BraVL (Du et al., 2023)	6.1	17.9	4.9	14.9	5.6	17.4	5.0	15.1	4.0	13.4	6.0	18.2	6.5	20.4	8.8	23.7	4.3	14.0	7.0	19.7	5.8	17.5
NICE	12.3	36.6	10.4	33.9	13.1	39.0	16.4	47.0	8.0	26.9	14.1	40.6	15.2	42.1	20.0	49.9	13.3	37.1	14.9	41.9	13.8	39.5
NICE-SA	13.3	40.2	12.1	36.1	15.3	39.6	15.9	49.0	9.8	34.4	14.2	42.4	17.9	43.6	18.2	50.2	14.4	38.7	16.0	42.8	14.7	41.7
NICE-GA	15.2	40.1	13.9	40.1	14.7	42.7	17.6	48.9	9.0	29.7	16.4	44.4	14.9	43.1	20.3	52.1	14.1	39.7	19.6	46.7	15.6	42.8
Subject independent - leave one subject out for test																						
BraVL (Du et al., 2023)	2.3	8.0	1.5	6.3	1.4	5.9	1.7	6.7	1.5	5.6	1.8	7.2	2.1	8.1	2.2	7.6	1.6	6.4	2.3	8.5	1.8	7.0
NICE	7.6	22.8	5.9	20.5	6.0	22.3	6.3	20.7	4.4	18.3	5.6	22.2	5.6	19.7	6.3	22.0	5.7	17.6	8.4	28.3	6.2	21.4
NICE-SA	7.0	22.6	6.6	23.2	7.5	23.7	5.4	21.4	6.4	22.2	7.5	22.5	3.8	19.1	8.5	24.4	7.4	22.3	9.8	29.6	7.0	23.1
NICE-GA	5.9	21.4	6.4	22.7	5.5	20.1	6.1	21.0	4.7	19.5	6.2	22.5	5.9	19.1	7.3	25.3	4.8	18.3	6.2	26.3	5.9	21.6

Table 3: Classification accuracy with different EEG encoder and Image encoder: top-1 (top-5)

Method	Subject 1	Subject 2	Subject 3	Subject 4	Subject 5	Subject 6	Subject 7	Subject 8	Subject 9	Subject 10	Ave	std
	EEG encoder											
ShallowNet (Schirrneister et al., 2017)	6.0 (16.0)	3.5 (21.5)	8.5 (28.0)	16.0 (41.0)	4.0 (16.5)	9.5 (32.0)	13.0 (31.0)	10.0 (24.5)	2.5 (9.0)	6.0 (22.5)	7.9 (24.2)	4.3 (9.3)
DeepNet (Schirrneister et al., 2017)	12.0 (31.0)	7.5 (27.5)	10.5 (33.0)	14.0 (36.5)	4.5 (20.0)	10.0 (33.0)	9.5 (30.0)	12.0 (41.0)	9.0 (31.5)	10.0 (33.5)	9.9 (31.7)	2.6 (5.5)
Conformer (Song et al., 2023)	11.0 (39.0)	8.5 (28.0)	11.0 (33.5)	14.5 (38.0)	6.0 (25.5)	10.0 (30.0)	13.0 (40.0)	13.0 (35.5)	10.5 (31.0)	13.5 (37.5)	11.1 (33.8)	2.6 (5.0)
EEGNet (Lawhern et al., 2018)	11.5 (38.0)	11.0 (35.5)	14.5 (37.5)	15.0 (43.5)	11.0 (30.0)	13.0 (42.5)	14.0 (35.5)	15.0 (42.5)	11.0 (37.0)	14.5 (41.5)	13.1 (38.4)	1.8 (4.2)
TSCov (ours)	12.3 (36.6)	10.4 (33.9)	13.1 (39.0)	16.4 (47.0)	8.0 (26.9)	14.1 (40.6)	15.2 (42.1)	20.0 (49.9)	13.3 (37.1)	14.9 (41.9)	13.8 (39.5)	3.3 (6.5)
Image encoder												
ResNet (He et al., 2016)	8.0 (13.0)	6.0 (11.0)	6.0 (11.5)	5.0 (9.5)	4.5 (10.0)	8.5 (12.0)	6.0 (10.5)	10.0 (14.5)	6.0 (12.0)	9.0 (13.5)	6.9 (11.8)	1.8 (1.6)
ViT (Dosovitskiy et al., 2021)	13.5 (27.0)	13.0 (28.5)	13.0 (29.0)	13.5 (32.5)	9.5 (21.5)	12.5 (29.0)	10.0 (34.0)	18.0 (38.5)	6.5 (24.5)	11.0 (29.5)	12.1 (29.4)	3.1 (4.8)
CLIP (Radford et al., 2021)	12.3 (36.6)	10.4 (33.9)	13.1 (39.0)	16.4 (47.0)	8.0 (26.9)	14.1 (40.6)	15.2 (42.1)	20.0 (49.9)	13.3 (37.1)	14.9 (41.9)	13.8 (39.5)	3.3 (6.5)

the results of the test set once after training. It takes about 5 minutes per subject to train with a batch size of 1000, since we get the image features in advance. The k in TSCov is set to 40, m_1 to 25, m_2 to 51, and s_2 to 5. Adam optimizer is used with the learning rate, β_1 and β_2 of 0.0002, 0.5, and 0.999, respectively. Wilcoxon Signed-Rank Test is employed to analyze the statistical significance.

4.3 OVERALL PERFORMANCE

The main results of our work are shown in Table 2. We trained the base framework (NICE), that with self-attention (NICE-SA), and with graph attention (NICE-GA) five times each for the averaged results. The evaluation was on the latest and most extensive image-EEG dataset, with only one state-of-the-art method BraVL for comparison (Du et al., 2023). The test set has 200 untrained image concepts, so it’s a 200-way zero-shot task with a chance level of 0.5%. Typical subject-dependent experiments were performed, training and testing on one subject. NICE has achieved better top-1 accuracy of 13.8% and top-5 accuracy of 39.5%, 8.0% and 22.0% higher than BraVL. The introduction of SA and GA improved the top-1 by 0.9% ($p < 0.05$) and 1.8% ($p < 0.01$), separately.

Besides, we conducted subject-independent experiments, leaving the test data of one subject in the test phase and using the training data of all the other subjects in the training phase. Our method still achieved top-1 of 6.2% and top-5 of 21.4%. However, NICE-SA improved the top-1 by 0.8% ($p > 0.05$), and NICE-GA only improved for several subjects, while the average top-1 decreased by 0.3%. We used base NICE for fair comparison in the following experiments.

4.4 ENCODER COMPARISON

The comparison of EEG encoders and image encoders is shown in Table 3. EEG encoder and image encoder are the necessary modules that affect the framework. We selected several representative methods based on convolutional neural networks and Transformer, including ShallowNet, DeepNet (Schirrneister et al., 2017), Conformer (Song et al., 2023), and EEGNet (Lawhern et al., 2018). TSCov was a concise network we designed with temporal and spatial convolution. The average top-1 accuracy of final adopted TSCov is 5.9% higher than ShallowNet ($p < 0.001$), 3.9% higher than DeepNet ($p < 0.001$), 2.7% higher than Conformer ($p < 0.001$), and 0.7% higher than EEGNet ($p > 0.05$). The robustness of TSCov reflected by standard deviation was not superior.

We utilized the model provided by huggingface, including ResNet-50 pre-trained on ImageNet-1k, ViT-B/16 pre-trained on ImageNet-21k and fine-tuned on ImageNet-1k, and CLIP-ViT-L/14 pre-trained on 400 million image-text pairs. CLIP pre-trained on huge amounts of data helped us achieve the highest results. Interestingly, ViT also worked well as the image encoder, with an average top-1 accuracy 1.7% lower than CLIP ($p > 0.05$). The results of ResNet were 6.9% lower ($p < 0.001$).

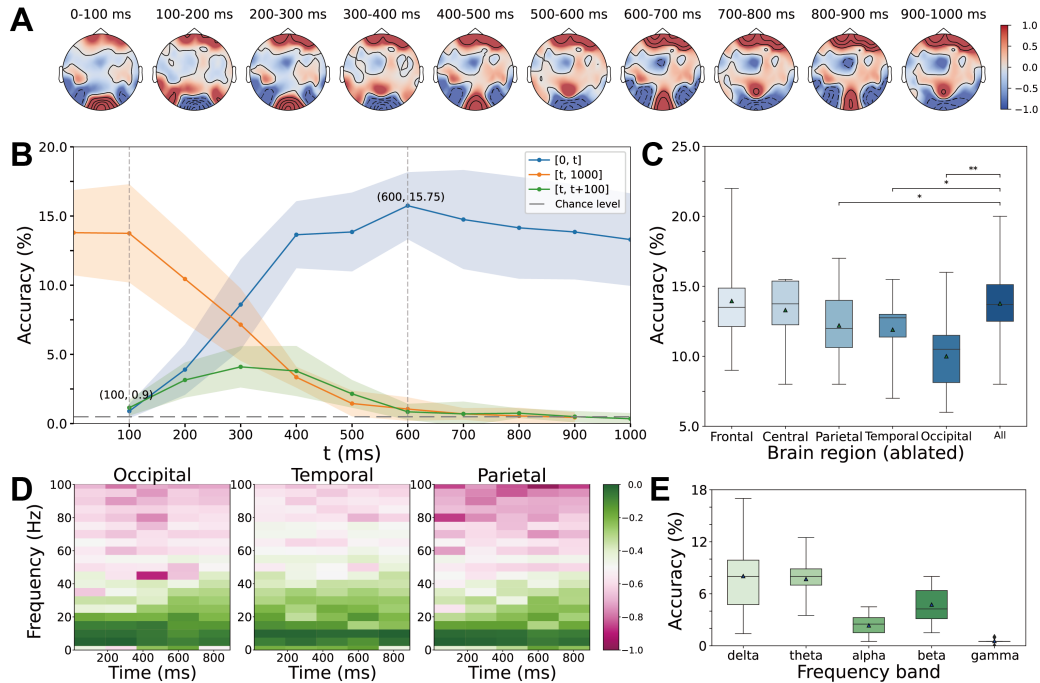


Figure 2: Temporal, spatial, spectral analysis. (A) Topographies of each 100 ms by averaging all training trials of one subject. The temporal lobe has a clear response between 100-600 ms. (B) Averaged accuracy of all subjects with different time lengths. The region of interest is 100-600 ms, after hysteresis in visual systems. (C) Ablate electrodes of different brain regions. The occipital, temporal, and parietal lobes contribute significantly to image decoding. (D) Time-frequency maps of the occipital, temporal, and parietal lobes data from one subject. The main components are below 30 Hz, and high-frequency components can be observed on the temporal lobe. (E) Averaged accuracy of different rhythms. Theta (~ 4 Hz) and beta ($\sim 14-18$ Hz) bands show effective performance.

4.5 TEMPORAL, SPATIAL, AND SPECTRAL DYNAMICS

Beyond the self-supervised framework, we try to demonstrate further that EEG can be used to decode images from our brain. We conducted a detailed analysis from the perspective of temporal, spatial, and spectral dynamics in Fig. 2. The topographies were first plotted with each 100 ms in Fig. 2(A) by averaging all training trials from the first subject. Visual masking (Keysers & Perrett, 2002) would be alleviated because the data used were collected in many rapid series sequences. A clear response could be observed on the temporal cortex in 100-600 ms after the stimulus, although the 200 ms stimulus onset asynchrony still caused periodic responses on the occipital cortex. Besides, the parietal cortex also had a response after 100 ms. The phenomenon is consistent with the bottom-up hierarchy of visual system (DiCarlo & Cox, 2007), that the visual stimulus is processed sequentially by the V1, V2, V4 on the occipital cortex, and inferotemporal (IT) on the temporal cortex along the ventral stream for object recognition (Bao et al., 2020).

We explored the active time range in three ways, incrementing forward, decrementing backward, and segmentation, as in Fig. 2(B). Data in the no concern range was set to zero. It could be seen that the region of interest was in 100 to 600 ms. The average top-1 accuracy of $[0, 1000]$ ms was 0.1% lower than that of $[100, 1000]$ ms without significance ($p > 0.05$). There was little useful information in the first 100 ms after onset, due to the hysteresis effect in the visual pathway before the information was processed (Kleinschmidt et al., 2002; Li et al., 2023; Sayal et al., 2020). The Original dataset research focused on the peaks at 110 ms (Gifford et al., 2022). Besides, the signal after 600 ms brought a negative effect, probably due to the noise from other stimuli and other cognitive processing, emerging a response increasing on the frontal lobe as in Fig. 2(A).

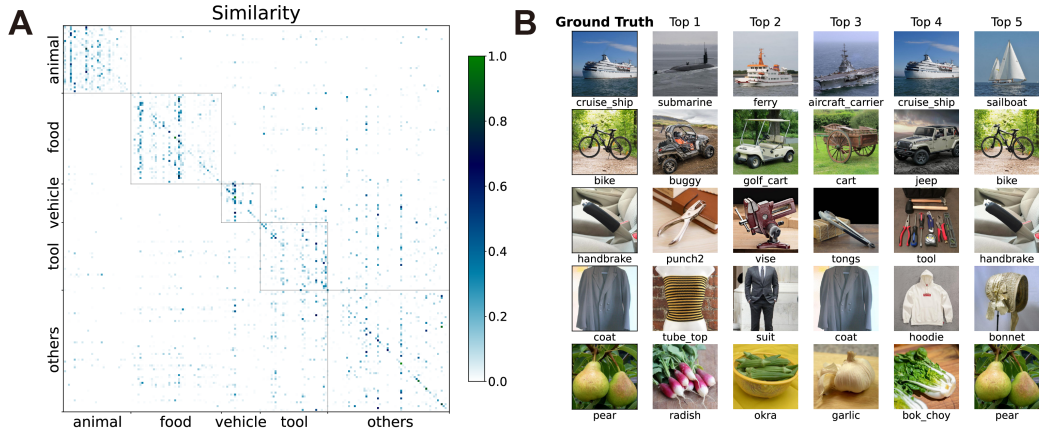


Figure 3: Semantic similarity analysis and visualization. (A) Cosine similarity of each image-EEG pair of 200 concepts in the test set. The results calculated by the trained models of 10 subjects were averaged, and all the concepts were rearranged into five categories, animal, food, vehicle, tool, and others. (B) Classification results visualized with ground truth (first column) and the top-5 predicted.

We performed an ablation study for the electrodes of different cortices as in Fig. 2(C). The average accuracy sharply declined 3.8% ($p < 0.01$) without occipital electrodes. Ablation of temporal, parietal electrodes and the central area near the motor cortex decreased the results by 1.9% ($p < 0.05$), 1.6% ($p < 0.05$), and 0.5% ($p > 0.05$) separately. The accuracy improved by 0.2% ($p > 0.05$) to discard frontal electrodes. The results are still reasonable, even with the low spatial resolution of EEG data.

We plotted time-frequency maps to show the frequency response in Fig. 2(D) by averaging all training trials from the first subject. The main components were below 30 Hz from the occipital, temporal, and parietal region data. High-frequency responses could be observed from electrodes on the temporal cortex. Interestingly, the frequency responses had an upward trend along with visual processing. The results are consistent with some known principles, that the bottom-up feedforward is carried by the synchronization of theta and gamma bands, and top-down feedback is influenced by beta and alpha band (Bastos et al., 2015; Michalareas et al., 2016).

We further conducted classification tests with different frequency bands in Fig. 2(E). Theta and delta bands near 4 Hz achieved good performance, where theta was more stable for different subjects. Beta and alpha bands also had a certain performance above the chance level, which was in line with previous results. However, the gamma band could hardly help us in decoding, for which we have two speculations. It's not easy to obtain pure gamma oscillations from EEG signals, due to the high frequency being susceptible to artifacts and noise (Fries et al., 2008; Yuval-Greenberg et al., 2008). Besides, the amplitude of the gamma band is very low and easily modulated by other cognitive processing, such as attention and memory (Herrmann & Demiralp, 2005). Some studies using MEG for image decoding have also neglected analysis of the gamma band (Hebart et al., 2023).

4.6 SEMANTIC SIMILARITY

We show the plausibility with semantic similarity and classification visualization in Fig. 3. One concern is that the discrimination we obtain from EEG is not due to semantic information but the images' color, brightness, contrast, etc. We calculated the cosine similarity between pairwise EEG and images processed by two encoders as the way of representational dissimilarity matrices (RDMs) (Cichy & Oliva, 2020). The similarity matrices of all subjects were averaged, and the 200 concepts in the test set were categorized into animal, food, vehicle, tool, and others. As shown in Fig. 3(A), we could observe distinct intra-category aggregation. This meant the obtained EEG representations were closer to the image representations within the corresponding semantic category.

The images in the test set were used for visualization in Fig. 3(B). We randomly chose several top-5 decoding results from the first subject. It could be noticed that the predicted results were semantically similar to the ground truth, such as the bike was predicted into several vehicles with wheels.

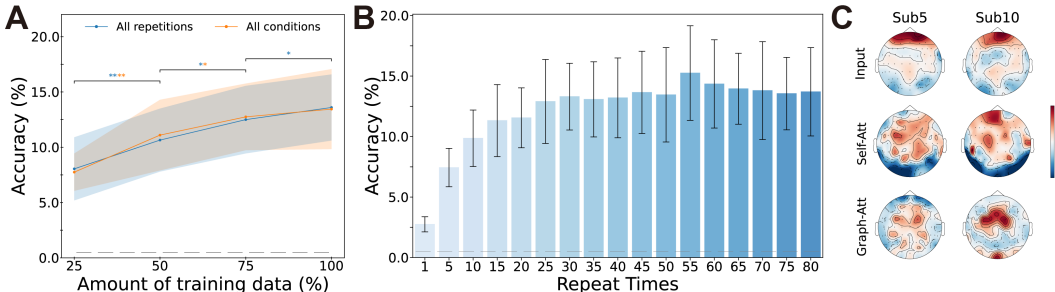


Figure 4: Effect of data size and repetition in training and test set, and visualization of self-attention and graph attention. (A) Accuracy with quarters of conditions and all repetitions, with quarters of repetitions and all conditions of training images. Adding more conditions has the potential to improve the performance further than more repetitions. (B) Accuracy with different repetitions of the test images. Average ten times to achieve an accuracy of 9.9% (30.1%), nearly takes 1 second. (C) Grad-CAM of self and graph attention. Activation on temporal and occipital regions could be seen.

4.7 DATA SIZE AND REPETITION

We compared the effect of the data size and repetition of the training and test sets, which may be crucial for the performance, as in Fig. 4. There were 1654 concepts \times 10 image conditions repeated four times in the training set. We averaged the four repetitions of each condition for training. Two cases were compared in Fig. 4(A), adding conditions by 25% intervals with all repetitions, and adding repetitions by 25% with all conditions. Increasing conditions, i.e., data size, contributed significantly to decoding accuracy from 25% to 50% ($p < 0.01$), from 50% to 75% ($p < 0.05$), and from 75% to 100% ($p < 0.05$). There were also significant contributions by increasing repetitions from 25% to 50% ($p < 0.01$), from 50% to 75% ($p < 0.05$), except from 75% to 100% ($p > 0.05$). The results suggest that increasing repetitions is of limited help, while more data promises further improvements.

From another view, repetitions of test data determine the practice efficiency. We compared the number of repetitions for averaging, from 5 to 80 with an interval of 5 in Fig. 4(B). Ten repetitions achieved a 9.9% (30.1%) accuracy, which tended to stabilize above 13.0% (37.0%) after twenty-five repetitions.

4.8 EFFECT OF SPATIAL MODULES

We tried to explain why the plug-in-play modules work, as in Fig. 4(C). Gradient-weighted class activation mapping (Grad-CAM) (Selvaraju et al., 2017) was used to visualize the interest region of SA and GA for spatial correlations. All the training data from the two subjects were used to show the topography. The original data was largely affected by the response on the frontal lobe. Surprisingly, self and graph attention helped the model focus on the temporal and occipital lobes.

5 DISCUSSION AND CONCLUSION

Researchers have worked on decoding visual activity from our brains for a long time. Some studies have achieved good results with fMRI but are still limited by expensive devices and seconds of time needed for one image (Horikawa & Kamitani, 2017; Shen et al., 2019). EEG is a viable alternative with low cost and high time resolution. However, prior studies have encountered experimental design pitfalls and limitations (Palazzo et al., 2021; Li et al., 2021). A large-scale EEG dataset was recently proposed to model human visual recognition and decode objects pairwise (Gifford et al., 2022).

Inspired by the rich dataset and the popular multi-modal learning, we propose a self-supervised framework to prove further the feasibility of decoding natural images from EEG. Contrastive learning aligned the features extracted from images and EEG signals. We achieved good results in the 200-way zero-shot image decoding. Furthermore, we got biological plausibility by analyzing time, space, frequency, and semantics. Our results were consistent with neuroscience principles.

There are also some limitations of this paper. Firstly, we have to use several repetitions for a stable response. That is probably because the 100 ms stimulus is very short, which is easy to be missed and disturbed by the stimuli before and after. We need to identify a more suitable window length in future work. Secondly, we have yet to capture useful information from the gamma band, which is supposed to be important for object recognition. Thirdly, the self and graph attention modules for spatial information need to be well-designed with some neural knowledge.

In conclusion, we propose a self-supervised framework to decode natural images from EEG with contrastive learning. Our framework has achieved remarkable results in zero-shot tasks with good biological plausibility. The results provide new inspiration for practical brain-computer interfaces.

REFERENCES

- Hamad Ahmed, Ronnie B. Wilbur, Hari M. Bharadwaj, and Jeffrey Mark Siskind. Object classification from randomized EEG trials. In *2021 IEEE/CVF Conference on Computer Vision and Pattern Recognition (CVPR)*, pp. 3844–3853, Nashville, TN, USA, June 2021. IEEE. ISBN 978-1-66544-509-2. doi: 10.1109/CVPR46437.2021.00384.
- Emily J. Allen, Ghislain St-Yves, Yihan Wu, Jesse L. Breedlove, Jacob S. Prince, Logan T. Dowdle, Matthias Nau, Brad Caron, Franco Pestilli, Ian Charest, J. Benjamin Hutchinson, Thomas Naselaris, and Kendrick Kay. A massive 7T fMRI dataset to bridge cognitive neuroscience and artificial intelligence. *Nature Neuroscience*, 25(1):116–126, January 2022. ISSN 1546-1726. doi: 10.1038/s41593-021-00962-x.
- Pinglei Bao, Liang She, Mason McGill, and Doris Y. Tsao. A map of object space in primate inferotemporal cortex. *Nature*, 583(7814):103–108, July 2020. ISSN 1476-4687. doi: 10.1038/s41586-020-2350-5.
- André Moraes Bastos, Julien Vezoli, Conrado Arturo Bosman, Jan-Mathijs Schoffelen, Robert Oostenveld, Jarrod Robert Dowdall, Peter De Weerd, Henry Kennedy, and Pascal Fries. Visual Areas Exert Feedforward and Feedback Influences through Distinct Frequency Channels. *Neuron*, 85(2):390–401, January 2015. ISSN 0896-6273. doi: 10.1016/j.neuron.2014.12.018.
- Xinyu Cheng, Wei Wei, Changde Du, Shuang Qiu, Sanli Tian, Xiaojun Ma, and Huiguang He. VigilanceNet: Decouple Intra- and Inter-Modality Learning for Multimodal Vigilance Estimation in RSVP-Based BCI. In *Proceedings of the 30th ACM International Conference on Multimedia*, pp. 209–217, Lisboa Portugal, October 2022. ACM. ISBN 978-1-4503-9203-7. doi: 10.1145/3503161.3548367.
- Radoslaw M. Cichy and Aude Oliva. A M/EEG-fMRI Fusion Primer: Resolving Human Brain Responses in Space and Time. *Neuron*, 107(5):772–781, September 2020. ISSN 0896-6273. doi: 10.1016/j.neuron.2020.07.001.
- Radoslaw Martin Cichy, Dimitrios Pantazis, and Aude Oliva. Resolving human object recognition in space and time. *Nature Neuroscience*, 17(3):455–462, March 2014. ISSN 1546-1726. doi: 10.1038/nn.3635.
- Djork-Arné Clevert, Thomas Unterthiner, and Sepp Hochreiter. Fast and accurate deep network learning by exponential linear units (elus). In *International Conference on Learning Representations*, 2016.
- Joel Dapello, Kohitij Kar, Martin Schrimpf, Robert Baldwin Geary, Michael Ferguson, David Daniel Cox, and James J. DiCarlo. Aligning Model and Macaque Inferior Temporal Cortex Representations Improves Model-to-Human Behavioral Alignment and Adversarial Robustness. In *The Eleventh International Conference on Learning Representations*, February 2023.
- James J. DiCarlo and David D. Cox. Untangling invariant object recognition. *Trends in Cognitive Sciences*, 11(8):333–341, August 2007. ISSN 1364-6613. doi: 10.1016/j.tics.2007.06.010.
- Yi Ding, Neethu Robinson, Chengxuan Tong, Qiuhaio Zeng, and Cuntai Guan. LGGNet: Learning From Local-Global-Graph Representations for Brain-Computer Interface. *IEEE Transactions on Neural Networks and Learning Systems*, pp. 1–14, 2023. ISSN 2162-2388. doi: 10.1109/TNNLS.2023.3236635.

- Alexey Dosovitskiy, Lucas Beyer, Alexander Kolesnikov, Dirk Weissenborn, Xiaohua Zhai, Thomas Unterthiner, Mostafa Dehghani, Matthias Minderer, Georg Heigold, Sylvain Gelly, Jakob Uszkoreit, and Neil Houlsby. An Image is Worth 16x16 Words: Transformers for Image Recognition at Scale. In *International Conference on Learning Representations*, April 2021.
- Changde Du, Changying Du, Lijie Huang, Haibao Wang, and Huiguang He. Structured Neural Decoding With Multitask Transfer Learning of Deep Neural Network Representations. *IEEE Transactions on Neural Networks and Learning Systems*, 33(2):600–614, February 2022. ISSN 2162-2388. doi: 10.1109/TNNLS.2020.3028167.
- Changde Du, Kaicheng Fu, Jinpeng Li, and Huiguang He. Decoding Visual Neural Representations by Multimodal Learning of Brain-Visual-Linguistic Features. *IEEE Transactions on Pattern Analysis and Machine Intelligence*, pp. 1–17, 2023. ISSN 1939-3539. doi: 10.1109/TPAMI.2023.3263181.
- Tao Fang, Yu Qi, and Gang Pan. Reconstructing Perceptive Images from Brain Activity by Shape-Semantic GAN. In *Advances in Neural Information Processing Systems*, volume 33, pp. 13038–13048. Curran Associates, Inc., 2020.
- Pascal Fries, René Scheeringa, and Robert Oostenveld. Finding Gamma. *Neuron*, 58(3):303–305, May 2008. ISSN 0896-6273. doi: 10.1016/j.neuron.2008.04.020.
- Kaicheng Fu, Changde Du, Shengpei Wang, and Huiguang He. Multi-View Multi-Label Fine-Grained Emotion Decoding From Human Brain Activity. *IEEE Transactions on Neural Networks and Learning Systems*, pp. 1–15, 2022. ISSN 2162-2388. doi: 10.1109/TNNLS.2022.3217767.
- Xiaorong Gao, Yijun Wang, Xiaogang Chen, and Shangkai Gao. Interface, interaction, and intelligence in generalized brain–computer interfaces. *Trends in Cognitive Sciences*, 25(8):671–684, August 2021. ISSN 1364-6613. doi: 10.1016/j.tics.2021.04.003.
- Alessandro T. Gifford, Kshitij Dwivedi, Gemma Roig, and Radoslaw M. Cichy. A large and rich EEG dataset for modeling human visual object recognition. *NeuroImage*, 264:119754, December 2022. ISSN 1053-8119. doi: 10.1016/j.neuroimage.2022.119754.
- Zijin Gu, Keith Wakefield Jamison, Meenakshi Khosla, Emily J. Allen, Yihan Wu, Ghislain St-Yves, Thomas Naselaris, Kendrick Kay, Mert R. Sabuncu, and Amy Kuceyeski. NeuroGen: Activation optimized image synthesis for discovery neuroscience. *NeuroImage*, 247:118812, February 2022. ISSN 1053-8119. doi: 10.1016/j.neuroimage.2021.118812.
- Matthias Guggenmos, Philipp Sterzer, and Radoslaw Martin Cichy. Multivariate pattern analysis for MEG: A comparison of dissimilarity measures. *NeuroImage*, 173:434–447, June 2018. ISSN 1053-8119. doi: 10.1016/j.neuroimage.2018.02.044.
- Kaiming He, Xiangyu Zhang, Shaoqing Ren, and Jian Sun. Deep Residual Learning for Image Recognition. In *2016 IEEE Conference on Computer Vision and Pattern Recognition (CVPR)*, pp. 770–778, Las Vegas, NV, USA, June 2016. IEEE. ISBN 978-1-4673-8851-1. doi: 10.1109/CVPR.2016.90.
- Martin N. Hebart, Adam H. Dickter, Alexis Kidder, Wan Y. Kwok, Anna Corriveau, Caitlin Van Wicklin, and Chris I. Baker. THINGS: A database of 1,854 object concepts and more than 26,000 naturalistic object images. *PLOS ONE*, 14(10):e0223792, 2019. ISSN 1932-6203. doi: 10.1371/journal.pone.0223792.
- Martin N Hebart, Oliver Contier, Lina Teichmann, Adam H Rockter, Charles Y Zheng, Alexis Kidder, Anna Corriveau, Maryam Vaziri-Pashkam, and Chris I Baker. THINGS-data, a multimodal collection of large-scale datasets for investigating object representations in human brain and behavior. *eLife*, 12:e82580, February 2023. ISSN 2050-084X. doi: 10.7554/eLife.82580.
- C. S. Herrmann and T. Demiralp. Human EEG gamma oscillations in neuropsychiatric disorders. *Clinical Neurophysiology*, 116(12):2719–2733, December 2005. ISSN 1388-2457. doi: 10.1016/j.clinph.2005.07.007.
- Jun Kai Ho, Tomoyasu Horikawa, Kei Majima, Fan Cheng, and Yukiyasu Kamitani. Inter-individual deep image reconstruction via hierarchical neural code conversion. *NeuroImage*, 271:120007, May 2023. ISSN 1053-8119. doi: 10.1016/j.neuroimage.2023.120007.

- Tomoyasu Horikawa and Yukiyasu Kamitani. Generic decoding of seen and imagined objects using hierarchical visual features. *Nature Communications*, 8(1):15037, May 2017. ISSN 2041-1723. doi: 10.1038/ncomms15037.
- Xiaoxuan Jia, Ha Hong, and James J DiCarlo. Unsupervised changes in core object recognition behavior are predicted by neural plasticity in inferior temporal cortex. *eLife*, 10:e60830, June 2021. ISSN 2050-084X. doi: 10.7554/eLife.60830.
- Yukiyasu Kamitani and Frank Tong. Decoding the visual and subjective contents of the human brain. *Nature Neuroscience*, 8(5):679–685, May 2005. ISSN 1546-1726. doi: 10.1038/nn1444.
- Kendrick N. Kay, Thomas Naselaris, Ryan J. Prenger, and Jack L. Gallant. Identifying natural images from human brain activity. *Nature*, 452(7185):352–355, March 2008. ISSN 1476-4687. doi: 10.1038/nature06713.
- Christian Keysers and David I Perrett. Visual masking and RSVP reveal neural competition. *Trends in Cognitive Sciences*, 6(3):120–125, March 2002. ISSN 1364-6613. doi: 10.1016/S1364-6613(00)01852-0.
- Andreas Kleinschmidt, Christian Büchel, Chloe Hutton, Karl J. Friston, and Richard S. J. Frackowiak. The neural structures expressing perceptual hysteresis in visual letter recognition. *Neuron*, 34(4):659–666, May 2002. ISSN 0896-6273. doi: 10.1016/s0896-6273(02)00694-3.
- Reinmar Kobler, Jun-ichiro Hirayama, Qibin Zhao, and Motoaki Kawanabe. SPD domain-specific batch normalization to crack interpretable unsupervised domain adaptation in EEG. *Advances in Neural Information Processing Systems*, 35:6219–6235, December 2022.
- Vernon J. Lawhern, Amelia J. Solon, Nicholas R. Waytowich, Stephen M. Gordon, Chou P. Hung, and Brent J. Lance. EEGNet: A compact convolutional neural network for EEG-based brain–computer interfaces. *Journal of Neural Engineering*, 15(5):056013, July 2018. ISSN 1741-2552. doi: 10.1088/1741-2552/aace8c.
- Ren Li, Jared S. Johansen, Hamad Ahmed, Thomas V. Ilyevsky, Ronnie B. Wilbur, Hari M. Bharadwaj, and Jeffrey Mark Siskind. The Perils and Pitfalls of Block Design for EEG Classification Experiments. *IEEE Transactions on Pattern Analysis and Machine Intelligence*, 43(1):316–333, January 2021. ISSN 1939-3539. doi: 10.1109/TPAMI.2020.2973153.
- Xiang Li, Jingjing Chen, Nanlin Shi, Chen Yang, Puze Gao, Xiaogang Chen, Yijun Wang, Shangkai Gao, and Xiaorong Gao. A hybrid steady-state visual evoked response-based brain-computer interface with MEG and EEG. *Expert Systems with Applications*, 223:119736, August 2023. ISSN 0957-4174. doi: 10.1016/j.eswa.2023.119736.
- Sikun Lin, Thomas Sprague, and Ambuj K Singh. Mind Reader: Reconstructing complex images from brain activities. In S. Koyejo, S. Mohamed, A. Agarwal, D. Belgrave, K. Cho, and A. Oh (eds.), *Advances in Neural Information Processing Systems*, volume 35, pp. 29624–29636. Curran Associates, Inc., 2022.
- Bingchuan Liu, Xiaogang Chen, Nanlin Shi, Yijun Wang, Shangkai Gao, and Xiaorong Gao. Improving the Performance of Individually Calibrated SSVEP-BCI by Task- Discriminant Component Analysis. *IEEE Transactions on Neural Systems and Rehabilitation Engineering*, 29:1998–2007, 2021. ISSN 1558-0210. doi: 10.1109/TNSRE.2021.3114340.
- Dongjun Liu, Weichen Dai, Hangkui Zhang, Xuanyu Jin, Jianting Cao, and Wanzeng Kong. Brain-Machine Coupled Learning Method for Facial Emotion Recognition. *IEEE Transactions on Pattern Analysis and Machine Intelligence*, pp. 1–15, 2023. ISSN 1939-3539. doi: 10.1109/TPAMI.2023.3257846.
- Georgios Michalareas, Julien Vezoli, Stan van Pelt, Jan-Mathijs Schoffelen, Henry Kennedy, and Pascal Fries. Alpha-Beta and Gamma Rhythms Subserve Feedback and Feedforward Influences among Human Visual Cortical Areas. *Neuron*, 89(2):384–397, January 2016. ISSN 0896-6273. doi: 10.1016/j.neuron.2015.12.018.

- Yoichi Miyawaki, Hajime Uchida, Okito Yamashita, Masa-aki Sato, Yusuke Morito, Hiroki C. Tanabe, Norihiro Sadato, and Yukiyasu Kamitani. Visual Image Reconstruction from Human Brain Activity using a Combination of Multiscale Local Image Decoders. *Neuron*, 60(5):915–929, December 2008. ISSN 0896-6273. doi: 10.1016/j.neuron.2008.11.004.
- Simone Palazzo, Concetto Spampinato, Isaak Kavasidis, Daniela Giordano, Joseph Schmidt, and Mubarak Shah. Decoding Brain Representations by Multimodal Learning of Neural Activity and Visual Features. *IEEE Transactions on Pattern Analysis and Machine Intelligence*, 43(11): 3833–3849, November 2021. ISSN 0162-8828. doi: 10.1109/TPAMI.2020.2995909.
- Yue-Ting Pan, Jing-Lun Chou, and Chun-Shu Wei. MAtt: A Manifold Attention Network for EEG Decoding. *Advances in Neural Information Processing Systems*, 35:31116–31129, December 2022.
- Alec Radford, Jong Wook Kim, Chris Hallacy, Aditya Ramesh, Gabriel Goh, Sandhini Agarwal, Girish Sastry, Amanda Askell, Pamela Mishkin, Jack Clark, et al. Learning transferable visual models from natural language supervision. In *International Conference on Machine Learning*, pp. 8748–8763. PMLR, 2021.
- Chitwan Saharia, William Chan, Saurabh Saxena, Lala Li, Jay Whang, Emily L Denton, Kamyar Ghasemipour, Raphael Gontijo Lopes, Burcu Karagol Ayan, Tim Salimans, Jonathan Ho, David J Fleet, and Mohammad Norouzi. Photorealistic text-to-image diffusion models with deep language understanding. In S. Koyejo, S. Mohamed, A. Agarwal, D. Belgrave, K. Cho, and A. Oh (eds.), *Advances in Neural Information Processing Systems*, volume 35, pp. 36479–36494. Curran Associates, Inc., 2022.
- Alexandre Sayal, Teresa Sousa, João V. Duarte, Gabriel N. Costa, Ricardo Martins, and Miguel Castelo-Branco. Identification of competing neural mechanisms underlying positive and negative perceptual hysteresis in the human visual system. *NeuroImage*, 221:117153, November 2020. ISSN 1053-8119. doi: 10.1016/j.neuroimage.2020.117153.
- Robin Tibor Schirrmeister, Jost Tobias Springenberg, Lukas Dominique Josef Fiederer, Martin Glasstetter, Katharina Eggenberger, Michael Tangermann, Frank Hutter, Wolfram Burgard, and Tonio Ball. Deep learning with convolutional neural networks for EEG decoding and visualization. *Human Brain Mapping*, 38(11):5391–5420, 2017. ISSN 1097-0193. doi: 10.1002/hbm.23730.
- Ramprasaath R. Selvaraju, Michael Cogswell, Abhishek Das, Ramakrishna Vedantam, Devi Parikh, and Dhruv Batra. Grad-CAM: Visual Explanations from Deep Networks via Gradient-Based Localization. In *2017 IEEE International Conference on Computer Vision (ICCV)*, pp. 618–626, October 2017. doi: 10.1109/ICCV.2017.74.
- Guohua Shen, Tomoyasu Horikawa, Kei Majima, and Yukiyasu Kamitani. Deep image reconstruction from human brain activity. *PLOS Computational Biology*, 15(1):e1006633, 2019. ISSN 1553-7358. doi: 10.1371/journal.pcbi.1006633.
- Nanlin Shi, Xiang Li, Bingchuan Liu, Chen Yang, Yijun Wang, and Xiaorong Gao. Representative-Based Cold Start for Adaptive SSVEP-BCI. *IEEE Transactions on Neural Systems and Rehabilitation Engineering*, 31:1521–1531, 2023. ISSN 1558-0210. doi: 10.1109/TNSRE.2023.3245654.
- Yonghao Song, Qingqing Zheng, Bingchuan Liu, and Xiaorong Gao. EEG Conformer: Convolutional Transformer for EEG Decoding and Visualization. *IEEE Transactions on Neural Systems and Rehabilitation Engineering*, 31:710–719, 2023. ISSN 1558-0210. doi: 10.1109/TNSRE.2022.3230250.
- C. Spampinato, S. Palazzo, I. Kavasidis, D. Giordano, N. Souly, and M. Shah. Deep Learning Human Mind for Automated Visual Classification. In *2017 IEEE Conference on Computer Vision and Pattern Recognition (CVPR)*, pp. 4503–4511, July 2017. doi: 10.1109/CVPR.2017.479.
- Yu Takagi and Shinji Nishimoto. High-resolution image reconstruction with latent diffusion models from human brain activity. *2023 IEEE Conference on Computer Vision and Pattern Recognition (CVPR)*, 2023.

- Ashish Vaswani, Noam Shazeer, Niki Parmar, Jakob Uszkoreit, Llion Jones, Aidan N Gomez, Łukasz Kaiser, and Illia Polosukhin. Attention is All you Need. In *Advances in Neural Information Processing Systems*, volume 30. Curran Associates, Inc., 2017.
- Petar Veličković, Guillem Cucurull, Arantxa Casanova, Adriana Romero, Pietro Liò, and Yoshua Bengio. Graph Attention Networks. In *International Conference on Learning Representations*, April 2018.
- Junke Wang, Dongdong Chen, Zuxuan Wu, Chong Luo, Luowei Zhou, Yucheng Zhao, Yujia Xie, Ce Liu, Yu-Gang Jiang, and Lu Yuan. OmniVL: One foundation model for image-language and video-language tasks. In S. Koyejo, S. Mohamed, A. Agarwal, D. Belgrave, K. Cho, and A. Oh (eds.), *Advances in Neural Information Processing Systems*, volume 35, pp. 5696–5710. Curran Associates, Inc., 2022.
- Francis R. Willett, Donald T. Avansino, Leigh R. Hochberg, Jaimie M. Henderson, and Krishna V. Shenoy. High-performance brain-to-text communication via handwriting. *Nature*, 593(7858): 249–254, May 2021. ISSN 1476-4687. doi: 10.1038/s41586-021-03506-2.
- Shlomit Yuval-Greenberg, Orr Tomer, Alon S. Keren, Israel Nelken, and Leon Y. Deouell. Transient Induced Gamma-Band Response in EEG as a Manifestation of Miniature Saccades. *Neuron*, 58(3): 429–441, May 2008. ISSN 0896-6273. doi: 10.1016/j.neuron.2008.03.027.
- He Zhao, Qingqing Zheng, Kai Ma, Huiqi Li, and Yefeng Zheng. Deep Representation-Based Domain Adaptation for Nonstationary EEG Classification. *IEEE Transactions on Neural Networks and Learning Systems*, 32(2):535–545, February 2021. ISSN 2162-2388. doi: 10.1109/TNNLS.2020.3010780.